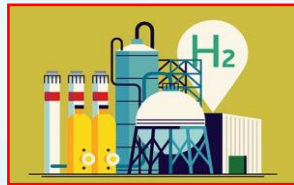
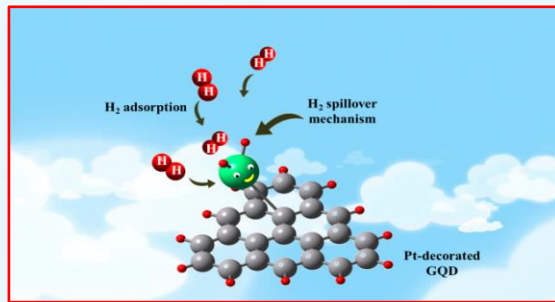


# Chapter 4

## Hydrogen Adsorption on Pristine and Platinum Decorated Graphene Quantum Dot



## **4.1 Introduction**

The much-needed and promising solution for energy crisis on Earth arises due to the excessive dependence on fossil fuels which can be overcome by developing clean, economical and renewable energy resources [1,2]. One of the best candidates, extensively considered and known for its low cost, non-polluting nature, and sustainability is hydrogen. However, the hydrogen has weak intermolecular interaction which is needed to be modified for its storage under ambient condition. Therefore, it has recently received countless attention in entire research society [3]. It is found both experimentally and theoretically that the hydrogen evolution reaction (HER) is a required electrochemical reaction for the utilization of hydrogen [4]. From intensive search, researchers found that the platinum (Pt) group metals show excellent HER performance as catalysts [5,6]. However, owing to their insufficiency and overprice, further development of the Pt based metal catalysts is enormously limited. There have been significant attempts in past years to explore novel materials that can be replaced or modified for improved hydrogen production [7-9]. Apart from the conventional leading factors, atomic arrangements and compositions of the materials, their low dimensional form has received tremendous attention in recent time [10-12]. Recently, a new class of low dimensional materials from the carbon group, a zero-dimensional member of graphene, graphene quantum dots (GQDs) having sized typically under 10nm have been discovered [13-17]. The GQDs have unique size and shape dependent photoluminescence (PL) and bandgap arising as a result of its edge effects and quantum confinement. Moreover, GQDs are less toxic with chemical inertness, bio-compatibility, and absence of photo-bleaching traits, endorsing its utilization in various areas, like biomedical, catalysis and photo-electronics [16,17]. For achieving the highest prospective of GQDs, intense studies have been done on GQDs-based nanocomposites with various noble metals like silver, palladium, aluminium and platinum [18-23]. Recently He et al. [23] observed an improved electrocatalytic activity in oxygen reduction reaction (ORR) with GQDs and platinum nanocomposites in contrast to the commercial Pt/C catalysts. In addition, for ecological, sustainable and affordable advancement of fuel cell systems, hydrogen storage stays to be the chief obstruction [24,25]. Ever since the discovery of carbon dependent materials, they have been known as proficient contenders for hydrogen storage [26-28]. In carbon materials, hydrogen can be stored through two adsorption approaches, physisorption and chemisorption, the former depends on feeble van der Waals

interaction while the latter is formed by the separation of hydrogen on carbon materials. Due to weak interaction the latter approach is the reversible, however, at ambient temperature, the high adsorption capacity of hydrogen molecule is improbable but it is essential for the experimental utilization [24]. For this significant development in hydrogen storage capability, doping of materials with slight amount of metals can be considered [28-31]. In a recent theoretical study of Yodsin et al. [32], platinum adsorbed carbon nanocone (Pt-CNC) shows significant hydrogen adsorption and diffusion. This kind of result arises due to Pt catalyst which efficiently influences hydrogen diffusion technique on carbon surface promoting the shift in hydrogen atom with energy barrier under 0.5 eV in ambient situations [32].

Polycyclic aromatic hydrocarbons (PAHs) can be obtained by cutting the graphene sheet into nano-fragments which creates various structures like pyrene, anthracene, triangulene, coronene, benzene and phenalenyl etc. and can be modeled as GQDs. Furthermore, their properties show similar properties like zero-dimensional nanographenes [33,34]. In some of the PAHs, ground state comprises closed-shell electronic configuration while others attain high spin, open-shell radical character [35,36]. These open shell PAHs are named as non-Kekulé polynuclear benzenoid attributed to topology of  $\pi$  electrons [34]. Recently for  $H_2$  formation, PAHs as catalyst has been proposed [37,38]. The study presents the interaction of hydrogen to pyrene PAH and interstellar medium hydrogen evolution along with site dependence [37].

The work presented in this chapter reports the potential of GQDs for hydrogen storage and HER [39]. The density functional theory calculations were performed for investigating the electronic properties and adsorption mechanism of GQDs. For the aforementioned, an open shell GQD i.e. triangulene ( $C_{22}H_{12}$ ) for HER is opted. Additionally, we have investigated site dependent adsorption process along with hydrogen storage, over Pt adsorbed triangulene. The considered sites for  $H_2$  interaction over triangulene are bridge denoted as “B”, hollow denoted as “H” and top denoted as “T”.

## **4.2 Computational methods**

The calculations for structural optimization and electronic properties of pristine and hydrogen absorbed GQD were done using Gaussian 09 program package [40]. The underlying theory is

spin-unrestricted density functional theory (DFT) where the exchange correlation functional was approximated by Becke three (B3) parameters hybrid functional by Lee-Yang-Perdew correlation functionals (LYP) owing to the triangulene's open-shell nature [41,42]. The hybrid functional results from mixing HF exchange by means of exchange correlation functional of Kohn Sham equation. The LANL2DZ basis set using effective core potential (ECP) was utilized for hydrogen molecule ( $H_2$ ) over Pt adsorbed triangulene. LANL2DZ describes D95V on first row [43], Los Alamos ECP plus DZ on Na-La and Hf-Bi [44,45]. The molecular orbitals obtained from DFT calculations were visualized using GaussView (version 5) [46] and density of states (DOS) plots were produced with Multiwfn software [47]. Absence of imaginary frequency was confirmed by calculations done at similar level as the structural and electronic. The adsorption sites chosen for platinum atom are: (i) over the center of carbon-carbon bond termed as bridge site (ii) over the center of hexagonal ring termed as hollow site and (iii) top of carbon atom termed as top site. The platinum adsorbed over bridge site, hollow site and top site triangulene are referred as "tri+Pt(B)", "tri+Pt(H)" and "tri+Pt(T)" respectively. The following equations calculated the adsorption energy ( $E_{ad}$ ) among the considered systems:

$$E_{ad} = E_{tri+pt} - (E_{tri} + E_{pt}) \quad (4.1)$$

$$E_{ad} = E_{tri+pt+H_2} - (E_{tri+pt} + E_{H_2}) \quad (4.2)$$

where  $E_{tri+pt}$  represents optimized energy of platinum adsorbed triangulene,  $E_{tri}$  and  $E_{H_2}$  are the optimized energies of pristine triangulene and hydrogen molecule respectively. The negative  $E_{ad}$  value expresses a stable adsorption complex over triangulene.

## **4.3 Results and discussion**

### **4.3.1 Hydrogen evolution reaction (HER)**

Initially, the structural properties of pristine and hydrogen adsorbed triangulene is determined. An open-shell PAH, triangulene molecule ( $C_{22}H_{12}$ ) existing in triplet ground state was synthesized recently [48] and has also been subjected to theoretical investigation [35]. The structural and electronic properties of both FM (triplet) and AFM (singlet) phases of triangulene are discussed in Chapter 3 and we have investigated that FM (triplet) state of triangulene is superior in stability [35]. Here, we will discuss electronic properties of pristine and hydrogen

adsorbed triangulene in its FM (triplet) states. The structure of triangulene with hydrogen used for initiating geometrical optimization is shown in Fig. 4.1(a). The hydrogen atom was placed at a distance of 2.50 Å above the carbon atom. The optimized geometry of hydrogen adsorbed triangulene is shown in Fig. 4.1(b). We confirmed the stability of optimized structure from all real vibrational frequencies during the ground-state calculation. The preferred position of hydrogen atom following adsorption is 3.66 Å above the carbon atom of triangulene (Fig. 4.1(b)) which can be attributed to the adsorption nature of GQD towards its edges.

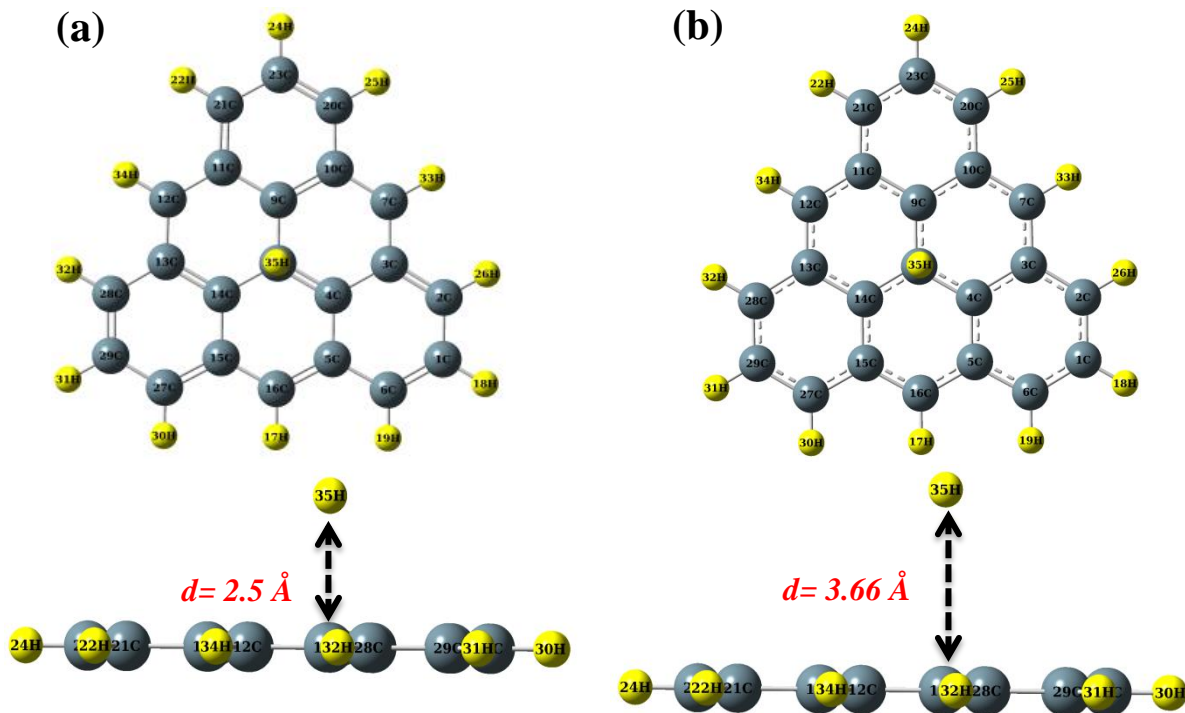


*Figure 4.1: (a) Initial and (b) optimized geometries of hydrogen atom over triangulene along with top and side views.*

To understand the performance of triangulene as a catalyst in HER, we analyzed the adsorption energy ( $E_{ad}$ ) of hydrogen using equation (4.1) and is presented in Table 4.1. The low  $E_{ad}$  value of -0.264 eV is better for the mechanism of hydrogen evolution reaction. We then calculated the site dependent adsorption energy of hydrogen where we found that the adsorption of hydrogen over the edges of GQD is -2.910 eV. Figure 4.2 presents both the initial and optimized configurations of hydrogen on the GQD edges.

*Table 4.1: Computed HOMO, LUMO, HOMO-LUMO gap ( $E_g$ ) and adsorption ( $E_{ad}$ ) energies of triangulene and hydrogen over triangulene.*

Systems	HOMO (eV)	LUMO (eV)	$E_g$ (eV)	$E_{ad}$ (eV)
Triangulene	-6.397	-2.664	3.73	-
triangulene+h	-6.389	-2.661	3.72	-0.264

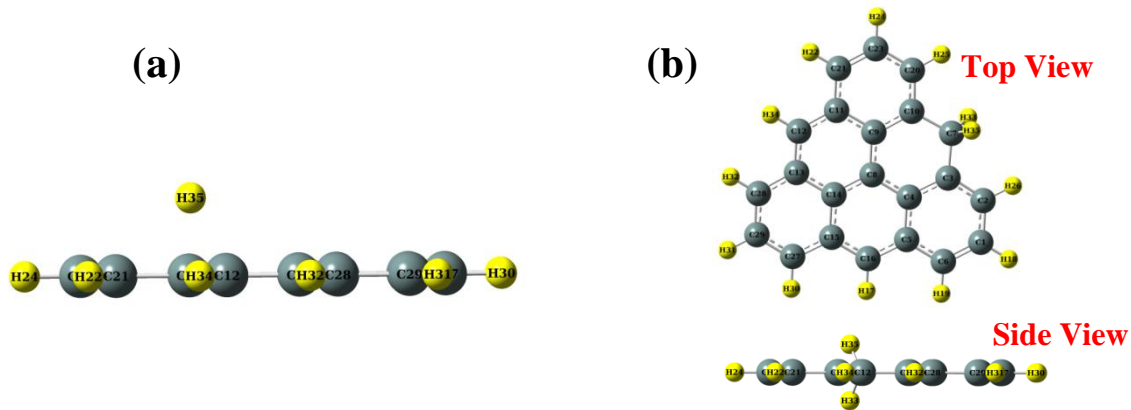


*Figure 4.2: (a) Side view of initial geometry of hydrogen over triangulene positioned at the edge and (b) optimized structure of hydrogen over edge of GQD depicting covalent interaction.*

Since, this high value is not suitable for HER, therefore, electronic properties of top site of GQD are evaluated only. Figure 4.3 shows the DOS of triangulene and triangulene+h. We observed subtle changes in the intrinsic band gap of triangulene on adsorption of hydrogen atom and is presented in Table 4.1. The energy bandgap ( $E_g$ ) is calculated using the following equation:

$$E_g = E_{LUMO} - E_{HOMO} \quad (4.3)$$

Figure 4.3 shows that the HOMO shifts slightly to the lower energy on adsorption of hydrogen, whereas LUMO is unaltered as evident from Table 4.1 which can be attributed to weak interaction of hydrogen with triangulene.

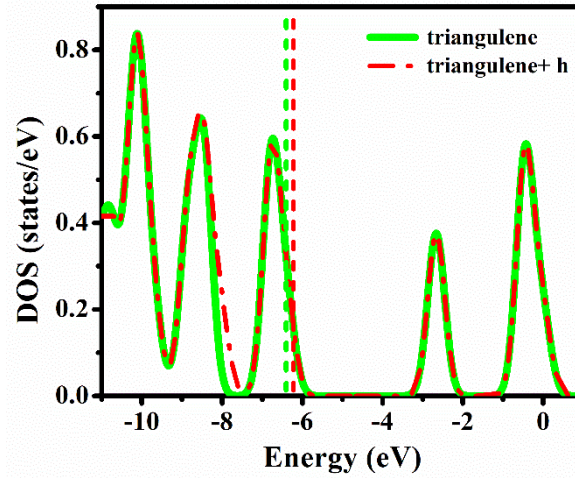


Figure 4.3: DOS of pristine triangulene and hydrogen over triangulene. The vertical dashed line presents the HOMO level energy.

We also calculated the charge transfer among hydrogen and triangulene and found that the transfer of charge is negligible ( $-3.75 \times 10^{-4} e$ ) confirming the results of our adsorption energy calculation. The HER comprises reduction of proton at the electrode resulting in production of hydrogen followed by  $H_2$  gas. The parameter determining the capability of surface in catalyzing the HER is the exchange current density which is further related to free energy of adsorbed hydrogen ( $H_2$ ) prior achieving the equilibrium state of reaction. The free energy of H in the adsorbed state is determined using the following equation:

$$\Delta G_{H^*} = E_{ad} + \Delta E_{ZPE} - T\Delta S_H \quad (4.4)$$

where  $\Delta E_{ZPE}$  denotes zero-point energy and  $E_{ad}$  denotes hydrogen adsorption in gaseous and adsorbed states. The zero point energy can vary between 0.0 to 0.04 eV [49-51]. The parameter  $T\Delta S_H$  is the change in entropy of hydrogen in same adsorbed and gaseous states which is experimentally determined to be -0.4 eV.  $H^*$  in the equation represents hydrogen adsorption. Considering the vibrational entropy to be negligible in the adsorbed state, one can show that the adsorption entropy of hydrogen is  $\Delta S_H \approx -1/2 \Delta S_H^O$ , where  $\Delta S_H^O$  is the entropy of hydrogen in gaseous state. We can therefore rewrite equation (4.4) as:  $\Delta G_{H^*} = \Delta E_{ad} + 0.24 eV$ , where  $\Delta G_{H^*}$  have to be zero to obtain worthy catalyst for hydrogen evolution reaction. Thus, we can predict

suitable candidate for HER from the adsorption energy values which should be near 0.24 eV. From Table 4.1, we can infer that triangulene is a promising candidate for HER with  $E_{ad}$  of -0.264 eV. Pristine triangulene presents superior HER functioning than other PAHs like pyrene and coronene as their  $E_{ad}$  ranges between 0.6-1.6 eV and 0.6-1.4 eV correspondingly [37]. Furthermore, our study suggests that pristine triangulene can perform better as catalyst in HER rather than platinum and palladium surfaces [52].

### 4.3.2 Hydrogen storage

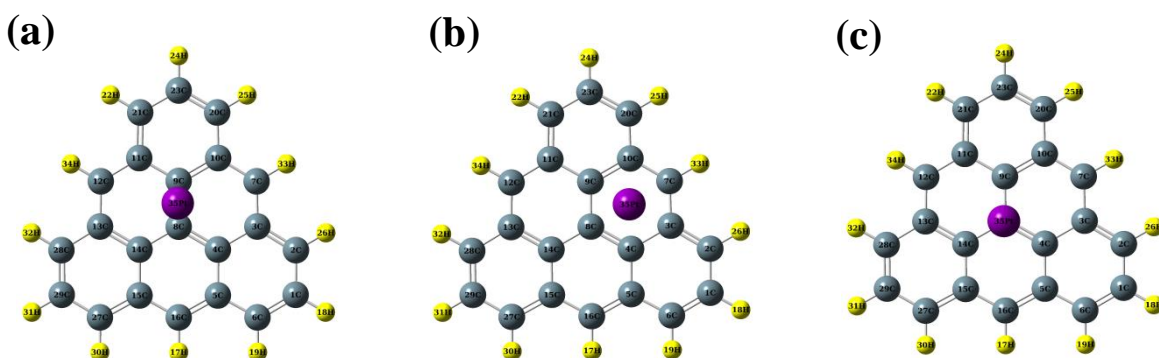


Figure 4.4: Initial geometries of Pt on triangulene with (a) bridge (b) hollow and (c) top sites.

To explore the hydrogen storage capability of triangulene, we initially performed adsorption of platinum with triangulene ( $C_{22}H_{12}$ ). Three adsorption sites were considered for Pt namely bridge, hollow and top sites. The top and side views of Pt adsorbed triangulene are presented in Figs. 4.4 (a-c). Pt atom was placed above the carbon atom at a distance of 2.50 Å across considered three sites, bridge site depicted as tri+Pt(B), hollow site depicted as tri+Pt(H) and top site depicted as tri+Pt(T). We confirmed the stability of all optimized structures by obtaining all real vibrational frequencies during the ground-state optimization calculations. The platinum atom placed at the bridge site of triangulene preferred in the company of carbon atom “9C” (numbering is depicted in Fig. 4.4). The optimized carbon and platinum (C-Pt) bond length is 2.14 Å, analogous to that obtained in platinum adsorption of graphene [53]. Likewise characteristics have been found in tri+Pt(T) with same bond length. Pt atom favors interaction on bridge site in both cases (bridge and top site).

Table 4.2: Calculated HOMO, LUMO,  $E_g$  and  $E_{ad}$  energies of all considered systems

System	tri+Pt (B)	tri+Pt (H)	tri+Pt (T)	tri+Pt+H <sub>2</sub> (B)	tri+Pt+ H <sub>2</sub> (H)	tri+Pt+ H <sub>2</sub> (T)
HOMO (eV)	-5.614	-5.418	-5.612	-5.77	-5.69	-5.77
LUMO (eV)	-2.844	-3.352	-2.844	-3.14	-3.16	-3.14
$E_g$ (eV)	2.32	2.06	2.31	2.63	2.53	2.63
$E_{ad}$ (eV)	-1.210	-1.994	-1.210	-2.029	-1.192	-2.029

In studying tri+Pt(H) system, Pt atom was seen to be adsorbed over the carbon atom “7C” with bond length of 2.05 Å. The results are summarized in Table 4.2 and Figs. 4.5(a-c) which show that the Pt atom undergoes chemisorption on all three bridge, hollow and top sites. This further concludes that the two unpaired electrons of triangulene and the open d-shell of platinum play an important role in their interaction.

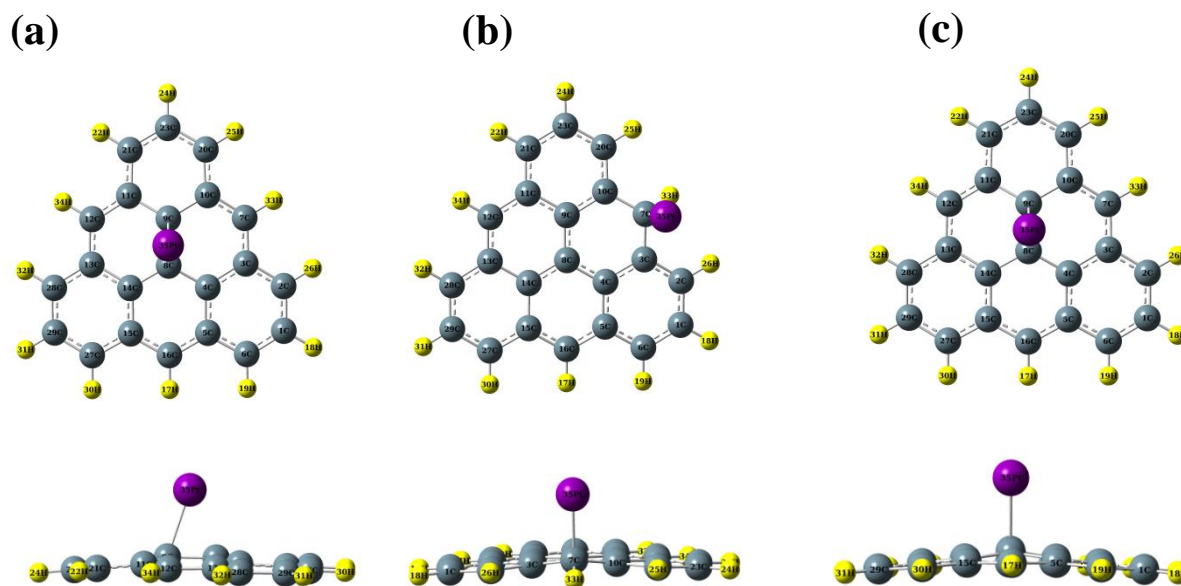
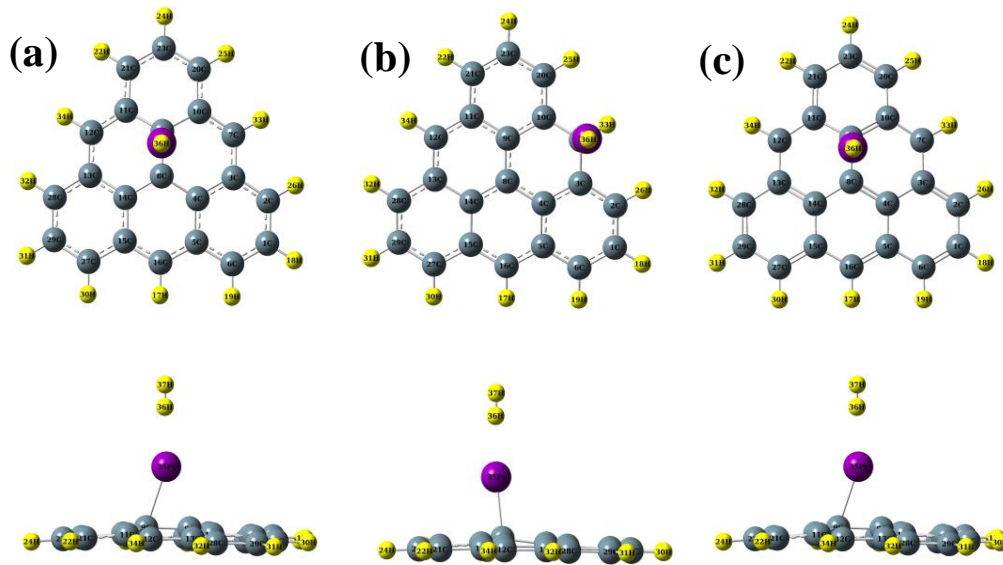


Figure 4.5: Optimized geometries of Pt adsorbed triangulene for sites (a) bridge (b) hollow and (c) top.

Further, we compare the adsorption energy of platinum on three considered adsorption sites. The highest adsorption energy of -1.994 eV was found for tri+Pt(H) whereas other two sites exhibit similar adsorption energy of -1.210 eV which can be attributed to the preference of platinum

atom towards the bridge site in consistent with that seen in the study of platinum adsorption in graphene [53]. It is also seen that the  $E_{ad}$  of Pt on triangulene is little higher than that over coronene [54]. The Fig. 4.6(a-c) shows the initial geometries considered to investigate hydrogen storage where  $H_2$  molecule is adsorbed on triangulene over all three considered bridge, hollow and top sites.



*Figure 4.6: Initial geometries of  $H_2$  on Pt adsorbed triangulene with different sites (a) bridge (b) hollow and (c) top.*

The optimized structures of  $H_2$  adsorbed triangulene decorated with platinum are shown in Fig. 4.7(a-c). The optimized H-H bond length is 1.90, 1.80 and 1.90 Å for sites tri+Pt+ $H_2$ (B), tri+Pt+ $H_2$ (H) and tri+Pt+ $H_2$ (T) respectively, which is found to be greater than its equilibrium bond length of 0.74 Å. Our calculations show that the Pt decorated triangulene can adsorb  $H_2$  molecule accompanied by  $H_2$  dissociation. Present study is in good agreement with previous investigations done on  $H_2$  over Pt adsorbed carbon dependent materials [28-31,54].

The tri+Pt+ $H_2$ (B) and tri+Pt+ $H_2$ (T) provide similar magnitude of  $E_{ad}$  which is equivalent to the adsorption behavior of Pt on triangulene. Apart from the similarity in the adsorption behavior, there is a significant difference in the structural properties between Pt with  $H_2$  and tri+Pt+ $H_2$ (B) and tri+Pt+ $H_2$ (T) systems due to different adsorption site. However the electronic properties are intact for tri+Pt+ $H_2$ (B) and tri+Pt+  $H_2$ (T).

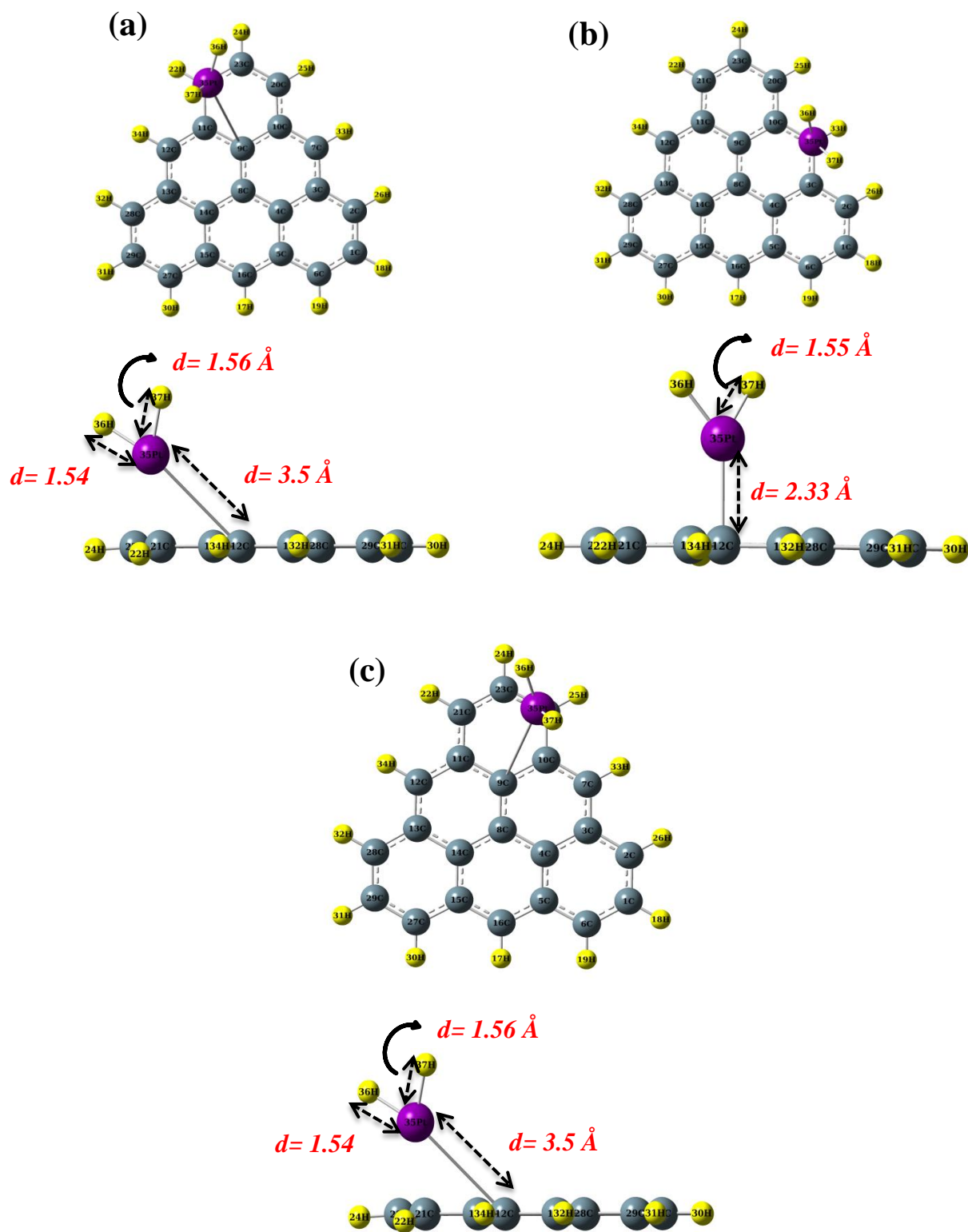


Figure 4.7: Optimized geometries of  $H_2$  on Pt adsorbed triangulene for all three sites (a) bridge (b) hollow and (c) top.

Fundamentally, the adsorption of  $H_2$  is categorized into two distinctive types in case of metal decorated carbon-based materials: first is the non-dissociative  $H_2$  adsorption, known as Kubas adsorption (K-mode), [55] and second is the dihydride adsorption where hydrogen is dissociated (D-mode) [56]. In this, we have observed the dissociation of  $H_2$  with Pt adsorbed GQD. In case of Ni, Pt, and Pd which are  $d^{10}$  transition metals, there are several studies reported on the stability of  $H_2$  adsorption on K- and D-modes carbon-based materials and its dependence on position and configuration [56-59]. Though, the  $H_2$  adsorption over Pt adsorbed triangulene results in D-mode in our study with all three considered sites such as bridge, hollow and top. The results regarding the  $E_{ad}$  are presented in Table 4.2 and the equation (4.2) is used to calculate the adsorption energy. The calculated adsorption energies are -2.029 eV for system tri+Pt+ $H_2$ (B), -1.192 eV for system tri+Pt+ $H_2$ (H) and -2.029 eV for system tri+Pt+ $H_2$ (T). Due to the similar structural properties in case of bridge and top sites, they present similar and maximum  $E_{ad}$  which corresponds with Pt adsorption over triangulene on both bridge and top sites.

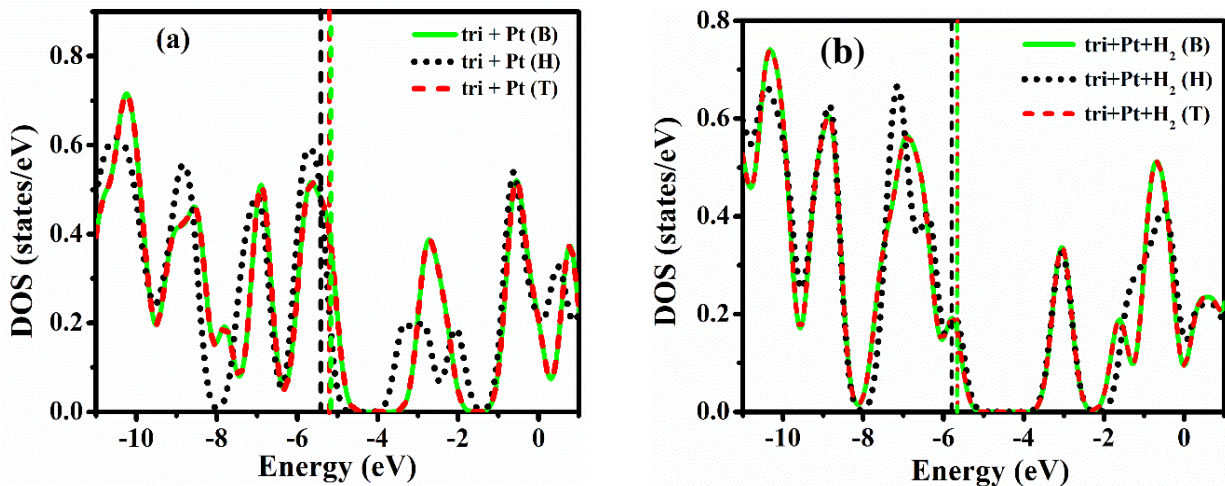


Figure 4.8: DOS of (a) Pt over triangulene (b)  $H_2$  on tri+Pt for all considered sites.

Our results suggest that GQDs are better material for metal supported hydrogen storage utilization. The DOS of Pt adsorbed over triangulene and  $H_2$  over Pt adsorbed triangulene is presented in Fig. 4.8(a-b). The bottom of the conduction band has main contribution of tri+Pt(H) rather than other sites. Increment in the HOMO level is observed (dash lines). In systems

tri+Pt(B) and tri+Pt(T), we observed perfect overlapping in the peaks of DOS, this can be attributed to the similar geometrical properties resulting in the similar electronic properties.

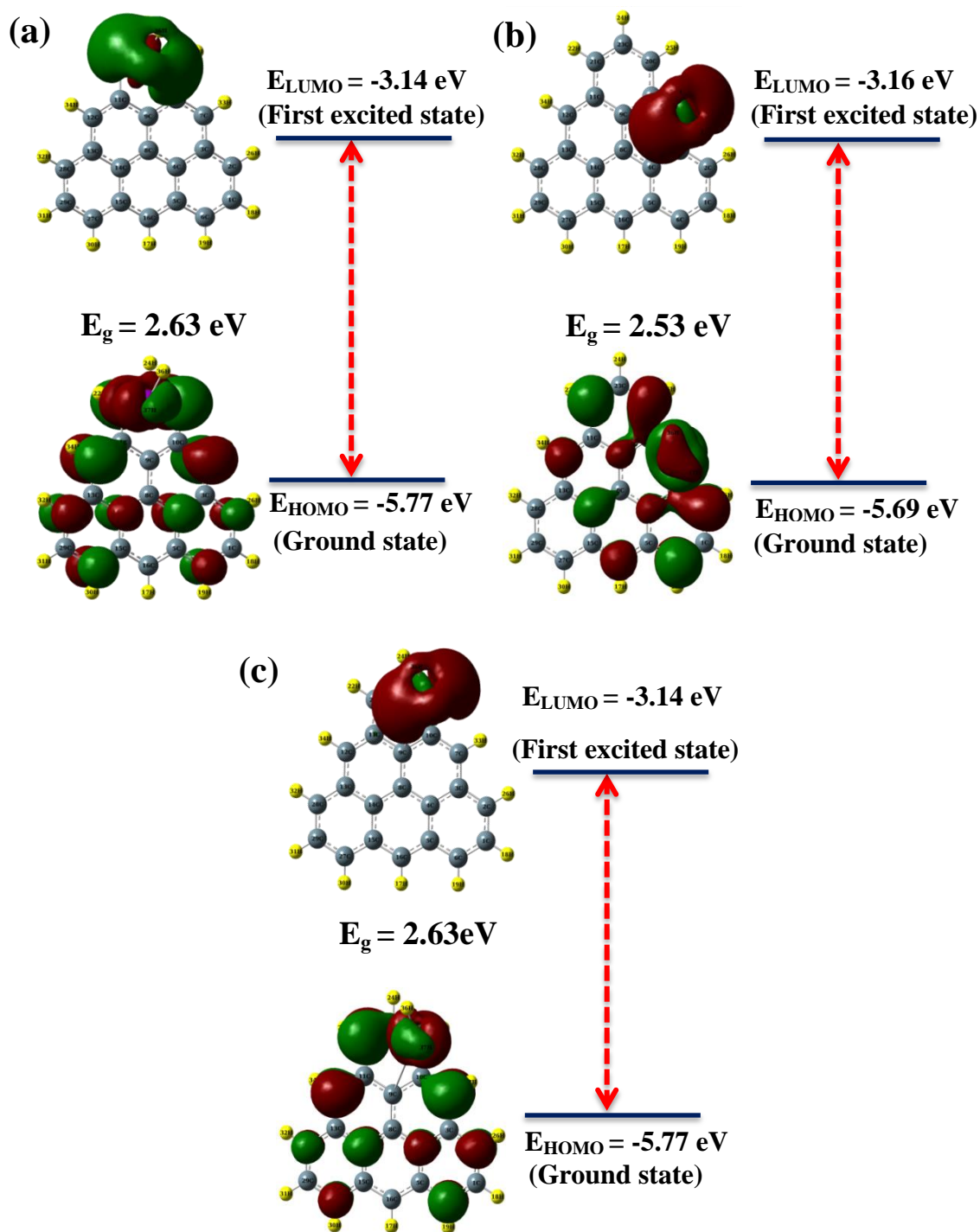


Figure 4.9: HOMO-LUMO surfaces of  $\text{H}_2$  over tri+Pt with (a) bridge, (b) hollow and (c) top sites.

Furthermore, after the adsorption of  $H_2$ , the conduction and valence bands are mainly dominated by  $tri+Pt+H_2$  (H), while similar peaks are observed in  $tri+Pt+H_2$ (B) and  $tri+Pt+H_2$ (T) systems. Figure 4.8(a-b) represents the HOMO levels which are shifted little in  $tri+Pt+H_2$ (B) and  $tri+Pt+H_2$ (T) systems. The FMO of interacting hydrogen adsorbed GQD systems are shown in Fig. 4.9(a-c) providing better understanding of the electronic properties. The HOMO orbitals are favorably localized at the hydrogen atom in all three considered systems, however, both Pt and triangulene shared the delocalized LUMO. The distribution for  $tri+Pt+H_2$ (B) and  $tri+Pt+H_2$ (T) of both HOMO and LUMO is same. The reason for the delocalization of LUMO and the formation of more homogeneous electron density distribution is equivalent. Our results show that the hydrogen can be stored on platinum adsorbed triangulene. Furthermore, present results will provide researchers in gaining the insight of following phase for hydrogen storage application i.e.  $H_2$  spillover mechanism into GQDs which is rather indistinguishable in experimental mechanisms.

#### 4.4 Conclusions

We studied the catalytic activity of triangulene in hydrogen evolution reaction using adsorption energy and electronic properties calculations. The top site of carbon atom is preferred by hydrogen on adsorption, however, the adsorption energy is very less. The low value of adsorption energy suggests its suitability for HER. The adsorption of hydrogen atom has little effect on electronic band gap of triangulene. Present study suggests that the triangulene can be used as a suitable electrocatalyst. The modification in structural and electronic properties as well as hydrogen storage property on platinum decoration is further studied. The preferred adsorption site by platinum is the hollow site of triangulene. The comprehensive site dependent analysis presents the potential of Pt decorated triangulene for possible application in hydrogen storage. Additionally, present results show better insight of  $H_2$  spill over mechanism in GQDs along with their design and synthesis for transition metal-GQDs for hydrogen storage.

#### References

1. J. A. Turner, *Science* **80** (2004) 972–974.
2. T. E. Mallouk, *Nat Chem* **5** (2013) 362–3.

3. H. Li, K. Wang, Y. Sun, C. T. Lollar, J. Li, H. C. Zhou, *Mater Today* **21** (2018) 108-121.
4. J. Greeley, T. F. Jaramillo, J. Bonde, I. Chorkendorff, J. K. Nørskov, *Nat Mater* **5** (2006) 909-913.
5. J. Greeley, I. E. L. Stephens, A. S. Bondarenko, T. P. Johansson, H. A. Hansen, T. F. Jaramillo et al. *Nat Chem* **1** (2009) 552-556.
6. Y. Yan B. Xia, Z. Xu, X. Wang, *ACS Catal.* **4** (2014) 1693.
7. G. Ye, Y. Gong, J. Lin, B. Li, Y. He, S. T. Pantelides et al., *Nano Lett* **16** (2016) 1097.
8. J. H. Montoya, M. Garcia-Mota, J. K. Nørskov, A. Vojvodic, *Phys Chem Chem Phys* **17** (2015) 2634.
9. M. S. Burke, L. J. Enman, A. S. Batchellor, S. Zou, S. W. Boettcher, *Chem Mater* **27** (2015) 7549.
10. S. B. Pillai, S. D. Dabhi, P. K. Jha, *Int J Hydrogen Energy* **43** (2018) 21649-21654.
11. N. N. Som, V. Mankad, P. K. Jha, *Int J Hydrogen Energy* **43** (2018) 21634-21641.
12. H. L. Kagdada, S. D. Dabhi, P. K. Jha, *Int J Hydrogen Energy* **43** (2018) 21724-21731.
13. K. Abinaya, S. Karthikaikumar, K. Sudha, S. Sundharamurthi, A. Elangovan, P. Kalimuthu, *Sol. Energy Mater. Sol. Cells* **185** (2018) 431.
14. L. Liu, K. Zheng, Y. Yan, Lin S. Cai, X. Hu, *Sol. Energy Mater. Sol. Cells* **185** (2018) 487.
15. J. Kusuma, R. G. Balakrishna, S. Patil, M. S. Jyothi, H. R. Chandan, Shwetharani, *Sol. Energy Mater. Sol. Cells* **185** (2018) 211.
16. J. Shen, Y. Zhu, X. Yang, C. Li, *Chem Commun* **48** (2012) 3686.
17. J. Shen, Y. Zhu, X. Yang, C. Li, *Nanoscale* **5** (2013) 4015-4039.
18. Z. S. Qian, X. Y. Shan, L. J. Chai, J. J. Ma, J. R. Chen, H. Feng, *Nanoscale* **6** (2014) 5671-5674.
19. L. Deng, L. Liu, C. Zhu, D. Li, S. Dong, *Chem Commun* **49** (2013) 2503-2505.
20. S. Chen, X. Hai, X. W. Chen, J. H. Wang, *Anal Chem* **86** (2014) 6689-6694.
21. C. Ran, M. Wang, W. Gao, Z. Yang, J. Shao, J. Deng, et al. *RSC Adv* **4** (2014) 21772-21776.
22. X. Yan, Q. Li, L.S. Li, *J Am Chem Soc* **134** (2012) 16095–16098.

- 
23. G. He, S. Chen, A. Walter, Y. Song, K. Liu, S. Chen, *ACS Catal* **3** (2013) 831–838.
  24. R. Ströbel, J. Garche, P.T. Moseley, L. Jörissen, G. Wolf, *J Power Sources* **159** (2006) 781.
  25. L. Wang, R. T. Yang, *Energy Environ Sci* **1** (2008) 268.
  26. A. Lueking, R. T. Yang, *AIChE J* **49** (2003) 1556-1568.
  27. V. Meregalli, M. Parrinello, *Appl Phys A Mater Sci Process* **72** (2001) 143.
  28. C. Rungnim, K. Faungnawakij, N. Sano, N. Kungwan, S. Namuangruk, *Int J Hydrogen Energy* **43** (2018) 23336-23345.
  29. J. R. Juarez-Mosqueda, A. Mavrandonakis, A. B. Kuc, L. G. M. Pettersson, T. Heine, *Front Chem* **3** (2015) 1-9.
  30. A. Soltani, M. B. Javan, M. S. Hoseininezhad-Namin, N. Tajabor, E. T. Lemeski, F. Pourarian, *Synth Met* **234** (2017) 1-8.
  31. F. Bakhshi, N. Farhadian, *Int J Hydrogen Energy* (2018) **43** 8355-8364.
  32. N. Yodsin, C. Rungnim, V. Promarak, S. Namuangruk, N. Kungwan, R. Rattanawan, et al., *Phys Chem Chem Phys* **20** (2018) 21194-21203.
  33. Y. Morita, S. Nishida. Phenalenyls, Cyclopentadienyls, and Other Carbon-Centered Radicals. In: Robin Hicks (Editor), editor. *Stable Radicals Fundam. Appl. Asp. Odd-Electron Compd.*, Wiley; 2010.
  34. E. Cair, The Significance of Double Bonds and Kekulé Structures for the Stability of Aromatic Systems. In: Clar E, editor. *Polycycl. Hydrocarb.*, Springer; 1964.
  35. V. Sharma, N. Som, S.D. Dabhi, P.K. Jha, *ChemistrySelect* **3** (2018) 2390-2397.
  36. V. Sharma, S. Narayan, S.D. Dabhi, S. Shinde, P.K. Jha, *AIP Conf. Proc.* **1961** (2018) 030031.
  37. J. A. Rasmussen, G. Henkelman, B. Hammer, *J Chem Phys* **134** (2011) 164703.
  38. V. Mennella, L. Hornekær, J. Thrower, M. Accolla, *Astrophys J Lett* **745** (2012) L2.
  39. V. Sharma, H. L. Kagdada, Jinlan Wang, P. K. Jha, *Int. J. Hydrog. Energy*. Doi: 10.1016/j.ijhydene.2019.09.021.
  40. M. J. Frisch, G. W. Trucks, H. B. Schlegel, G. E. Scuseria, M. A. Robb, J. R. Cheeseman et al., *Gaussian 09 C.01*. Gaussian, Inc Wallingford CT 2010.

- 
41. A. D. Becke, *Phys Rev A* **38** (1988) 3098.
  42. C. Lee, W. Yang, R. G. Parr, *Phys Rev B* **37** (1988) 785.
  43. T. H. Dunning Jr., P. J. Hay, Gaussian Basis Sets for Molecular Calculations. In: H. F. Schaefer, editor. *Methods Electron. Struct. Theory*, Springer; 1977, p. 1–28.
  44. P. J. Hay, W. R. Wadt, *J Chem Phys* **82** (1985) 270-283.
  45. W. R. Wadt, P. J. Hay, *J Chem Phys* **82** (1985) 284-298.
  46. R. Dennington, T. Keith, J. Millam, Gaussview, Version 5. Semichem Inc, Shawnee Mission KS:Semichem Inc 2016.
  47. T. Lu, F. Chen, *J Comput Chem* **33** (2012) 580-592.
  48. N. Pavliček, A. Mistry, Z. Majzik, N. Moll, G. Meyer, D. J. Fox et al., *Nat Nanotechnol* **12** (2017) 308-311.
  49. J. K. Nørskov, U. Stimming, S. Pandalov, J. R. Kitchin, J. G. Chen, A. Logadottir et al. *J Electrochem Soc* **152** (2005) J23.
  50. T. L. Tan, L. L. Wang, D. D. Johnson, K. Bai, *Nano Lett* **12** (2012) 4875.
  51. Y. Wang, S. L. Shang, H. Fang, Z. K. Liu, L. Q. Chen, *Npj Comput Mater* **2** (2016) 16006.
  52. I. A. Pašti, N. M. Gavrilov, S. V. Mentus, *Adv Phys Chem* **2011** (2011) 305634.
  53. Y. Tang, Z. Yang, X. Dai, *J Chem Phys* **135** (2011) 224704.
  54. G. M. Psofogiannakis, G. E. Froudakis, *J Phys Chem C* **113** (2009) 14908-14915.
  55. J. K. Gregory, *Acc Chem Res* **21** (1988) 120–128.
  56. H. Valencia, A. Gil, G. Frapper, *J Phys Chem C* **119** (2015) 5506-5522.
  57. I. López-Corral, J. De Celis, A. Juan, B. Irigoyen, *Int J Hydrogen Energy* **37** (2012) 10156-10164.
  58. Q. Zhou, C. Wang, Z. Fu, L. Yuan, X. Yang, Y. Tang et al., *Int J Hydrogen Energy* **40** (2015) 2473-2483.
  59. S. Seenithurai, R. K. Pandyan, S. V. Kumar, M. Mahendran, *Int J Hydrogen Energy* **38** (2013) 7376-7381.